Patient-specific numerical simulation of stent-graft deployment: Validation on three clinical cases.

David Perrin, Pierre Badel, Laurent Orgéas, Christian Geindreau, Aurélien Dumenil, Jean-Noël Albertini, Stéphane Avril

Patient-specific numerical simulation of stent-graft deployment: validation on three clinical cases

David PERRIN[1,2,3], Pierre BADEL[1], Laurent ORGEAS[2,3], Christian GEINDREAU[2,3], Aurélien DUMENIL[4,5,6], Jean-Noël ALBERTINI[7,8], Stéphane AVRIL[1]

[1] Ecole Nationale Supérieure des Mines de Saint-Etienne, CIS-EMSE, CNRS:UMR5307, LGF, F-42023 Saint-Etienne, France

[2] CNRS, 3SR Lab, F-38000 Grenoble, France

[3] Univ. Grenoble Alpes, 3SR Lab, F-38000 Grenoble, France

[4] INSERM, U1099, F-35000 Rennes, France

[5] Université de Rennes 1, LTSI, F-35000 Rennes, France

[6] Therenva, F-35000 Rennes, France

[7] CHU Hôpital Nord Saint-Etienne, Department of CardioVascular Surgery, Saint-Etienne F-42055, France

[8] Université Jean Monnet, GRT EA 3065, Saint-Etienne F-42023, France

Corresponding author:

Stéphane Avril

Center for Biomedical and Healthcare Engineering, Ecole Nationale Supérieure des Mines de Saint-Etienne

158 cours Fauriel, CS 62362, 42023 SAINT-ETIENNE CEDEX 2 France

Phone: +33477420188, Fax: +33477499755, Email: avril@emse.fr

Keywords: endovascular repair, abdominal aortic aneurysm, stent-graft, patient-specific, finite-element analysis

Abstract

Endovascular repair of abdominal aortic aneurysms faces some adverse outcomes, such as kinks or endoleaks related to incomplete stent apposition, which are difficult to predict and which restrain its use although it is less invasive than open surgery. Finite element simulations could help to predict and anticipate possible complications biomechanically induced, thus enhancing practitioners' stent-graft sizing and surgery planning, and giving indications on patient eligibility to endovascular repair. The purpose of this work is therefore to develop a new numerical methodology to predict stent-graft final deployed shapes after surgery. The simulation process was applied on three clinical cases, using preoperative scans to generate patient-specific vessel models. The marketed devices deployed during the surgery, consisting of a main body and one or more iliac limbs or extensions, were modeled and their deployment inside the corresponding patient aneurysm was simulated. The numerical results were compared to the actual deployed geometry of the stent-grafts after surgery that was extracted from postoperative scans. We observed relevant matching between simulated and actual deployed stent-graft geometries, especially for proximal and distal stents outside the aneurysm sac which are particularly important for practitioners. Stent locations along the vessel centerlines in the three simulations were always within a few millimeters to actual stents locations. This good agreement between numerical results and clinical cases makes finite element simulation very promising for preoperative planning of endovascular repair.

Introduction

Rupture of abdominal aortic aneurysm (AAA) is the primary cause of death of over 10,000 people in the United States each year (Kochanek et al., 2011). Prevention of AAA rupture is achieved either by open surgery or endovascular repair (EVAR). EVAR is associated with reduced postoperative mortality and morbidity compared to conventional surgery. However, the incidence of aneurysm related secondary procedures remains higher following EVAR than after open repair (Greenhalgh et al., 2010).

Endoleaks and stent-graft (SG) limb thrombosis are among the most frequent causes of secondary interventions following EVAR. Endoleaks may be associated with incomplete SG apposition on the arterial wall (Albertini et al., 2001, 2005). Graft kinking has been proved to favor stenosis and thrombosis (Carroccio et al., 2002; Cochennec et al., 2007). Highly tortuous and stiff calcified arteries are commonly associated to difficult outcomes (Albertini et al., 2006; Sternbergh et al., 2002).Therefore, mechanical behaviors of both SG and arterial wall appear to play an important role in the pathophysiology of these complications.

Within this context, finite-element analysis (FEA) could help predicting SG positioning inside patient-specific AAA, thus enabling surgeons to anticipate complications. Several teams have started to investigate this promising research field. Some of them focused on EVAR long term outcomes through fluid dynamics (Figueroa et al., 2010; Georgakarakos et al., 2014; Howell et al., 2007) and fluid-structure interactions to estimate the blood mechanical action onto SGs (Layman et al., 2010; Li and Kleinstreuer, 2006; Molony et al., 2010; Prasad et al., 2013). Despite their major interest, these studies present the following limitations: (i) they do not take into account SG deployment and (ii) most of them use oversimplified SG models, with a single equivalent homogenous mechanical behavior. Other groups investigated stent mechanics and their deployment in arteries (Auricchio et al., 2011; Holzapfel et al., 2005; Mortier et al., 2010). Following these pioneering studies, a number of researchers (De Bock et al., 2013; Kleinstreuer et al., 2008) have used FEA to model stent-graft structures, with both stents and graft mechanical behaviors. Our group recently achieved similar simulations (Demanget et al., 2013, 2012a) on several marketed SG limbs, which were validated against *in-vitro* bending tests (Demanget et al., 2012b). A step further has consisted in simulating SG deployment in aneurysm models. We developed simulations of SG deployment in idealized iliac aneurysm models (Perrin et al., 2015). De Bock et al. (2012) performed a SG deployment inside a silicone model and compared simulated and *in-vitro* SG positions. Auricchio et al. (2013) simulated the deployment of a custom-made tube aortic SG inside the

corresponding patient-specific aneurysm model. Each of the above mentioned studies had limitations. The first one did not model patient-specific aneurysms and the second did not validate the simulation against *in-vivo* data. The third study simulated a tubular custom-made SG, much simpler than the bifurcated manufactured SGs usually used to treat AAAs. .

The objective of the present study was to develop a FE methodology to simulate the deployment of marketed bifurcated SGs in patient-specific aneurysm models. In order to reduce computational costs, an original morphing technique was developed to simulate SG deployment.

Methods

Clinical summary

Three patients were included in this study after informed consent and approval from the Institutional Review Board. Patients, SGs and aorto-iliac characteristics are reported in Table 1. The devices were marketed by Medtronic (Santa Rosa, CA, USA) except for one right limb in clinical case #2 made by Cook Medical (Bloomington, Indiana, USA). Pre-operative and one-month post-operative computed tomography angiography (CTA) scans were available for all patients.

Vessel geometries and constitutive modeling

Surgery oriented Endosize® software (Therenva, France) was used to extract aortic and iliac vessel centerlines and vascular lumen contours from pre-operative scans (Kaladji et al., 2013). Centerlines of the arteries were constituted of a set of points, spaced by 5 mm to obtain a smooth centerline interpolation, onto which were centered B-splines describing the vascular lumen contour. Each B-spline had 10 control points on the lumen surface, in each plane orthogonal to the centerline. The continuous geometry of lumen surface was generated by surface interpolation driven by the B-splines in ANSYS DesignModeler software (ANSYS, Inc., Canonsburg, PA). The arterial lumen surface was then meshed

with 3-node linear shell elements (1.5 mm mean edge length) with 1.5 mm and 1.0 mm thicknesses for aortic and iliac surfaces, respectively. 3D pre-operative scans (A) and corresponding triangular meshes (B) are shown in Fig.1.

Assuming that SG deployment induced small strains within the arterial wall, the latter was modeled as an orthotropic linear elastic material. In-plane mechanical parameters were computed by linearizing, throughout the physiological range of pressures, Holzapfel-Gasser-Ogden anisotropic hyperelastic model (Gasser et al., 2006), with parameter values obtained for above 61 year-old patient abdominal aortas by Haskett et al. (2010). For that purpose, a hyperelastic pipe (20 mm diameter, 1.5 mm thickness, 100 mm length) was subjected to *in-vivo* loading conditions (100 mmHg internal pressure and 10% longitudinal stretch (Horný et al., 2013)). Then, the tangent stiffness matrix around these *in-vivo* conditions was derived by subjecting the pipe to different loading increments: pressure (5 mmHg), twist (2°) or longitudinal displacements (0.2 mm). The longitudinal, circumferential and shear elastic moduli, along with the Poisson ratio were obtained from the results of these simulations. The same value as in-plane shear modulus was chosen for the transverse shear moduli. The parameters of the hyperelastic model and the linearized elastic moduli are reported in Table 2.

Stent-graft modeling

Digitized geometries of SG main bodies and limbs were provided by the manufacturer, except the Cook Medical limb whose model had been validated in Demanget et al. (2012b), the dimensions of which were scaled to the current clinical case. Stents were meshed with linear beam elements (0.075 mm mean length). The superelastic behavior of Nitinol stents was modeled with Auricchio's model (Auricchio and Taylor, 1997) and implemented in a subroutine included in FEA software Abaqus (Simulia, Dassault Systems, Providence, RI, USA). The constitutive parameters of Nitinol, in the range of literature values, were provided by the manufacturer. Grafts were meshed with linear 4-node shell elements (0.4 mm

mean edge length). Polyester fabric was modeled as an orthotropic elastic material. In-plane and bending stiffness characterized in a previous study of our group (Demanget et al., 2012a) were used.

During SG manufacturing process, expanded stents diameters are oversized compared to graft diameters. For Medtronic components, a preliminary FEA was performed to tie the oversized stents to the graft. For the Cook limb, Z-stents were not oversized and modeled according to Demanget et al. (2012b).. The resulting pre-stressed SG models are depicted in Fig.1C.

Simulation methodology

A major challenge of simulating SG deployment in patient-specific models of aneurysm is to find appropriate boundary conditions for SG introduction. Our methodology, although different from the actual surgical procedure, has the potential to be used for any SG model and any aneurysm model. Also, it avoids simulating the full crimping and progressive deployment of the SG which are time expensive and may lead to numerical instabilities. A detailed description of the four steps of our simulation, which are described hereafter, is provided in Appendix A.

The main body, the iliac limbs and extensions were first compressed radially (slight crimping stage) and assembled (Fig.2A). Then, the assembled SG was inserted inside a virtual tubular shell (Fig.2B). From this configuration, proper displacements were prescribed onto the nodes of the virtual shell to morph its geometry onto the pre-operative geometry of the patient's aneurysm while prescribing contact to maintain the SG inside the shell. Note that, during this step, the shell did not present any mechanical behavior and only acted as a geometrical constraint. At the end of this step, the deployment of the SG inside the pre-operative geometry of the AAA was simulated (Fig.2C). Finally, the shell elements were ascribed the linearized AAA mechanical properties and all the boundary conditions previously assigned onto the AAA were released, for the SG to recoil and deform the vascular lumen until reaching static mechanical equilibrium (Fig.2D). Only proximal and distal ends of the vessels remained clamped.

All simulations were carried out with the explicit FE solver of Abaqus v6.12 software. Time increments (adjusted via mass scaling) and time steps (Table 3) were chosen to obtain fast results while keeping the ratio of kinematic and internal energies under 10% to avoid spurious dynamic effects, as shown in Fig.3. The FE simulations were run on 12 CPUs computers, 2.66GHz, 24 GB RAM.

Contacts were modeled using the general penalty algorithm implemented in Abaqus, with standard Coulomb friction law. The friction coefficient was set to 0.4, i.e. in the range of literature values (Vad et al., 2010).

Model validation methodology

Post-operative scan registration and stent segmentation

To validate the simulations, post-operative scans following EVAR procedures were used to quantify the position error of the simulated SGs. The voxel sizes of the three patient scans were respectively $0.85x0.85x0.625mm^3$, $0.76x0.76x0.7mm^3$ and $0.85x0.85x0.7mm^3$. Firstly, rigid image registration was used to align post-operative and pre-operative scans in the same coordinate system. Ten anatomical landmarks were picked on iliac bones, vertebras and vessel calcifications far from the surgical area, on each set of pre-operative and post-operative CTAs. A Matlab® function based on the iterative closest point method was used for the rigid registration. After this procedure, the mean distance between registered pre-operative points and post-operative points was 2.0 ± 1.2 mm.

Therefrom, stent centerlines were segmented by manually picking the center of stent cross-sections on each slice of the post-operative scans (Fig.4A). Stents located in overlap regions or in areas where vessels were highly calcified could not be properly segmented and were not considered in the validation process.

Cylinder fitting on stents

In the three registered simulation results and post-operative CTAs, a cylinder was defined for each stent using a Matlab® routine, so that the distance from stent points to the cylinder surface was minimal. For example, Fig.4B shows cylinders fitted on case #3 post-operative stents. In order to gauge the relevance of the simulations, radius and cylinder center position were compared between registered simulations and post-operative scans. For each simulated stent, diameter error e_D was estimated and normalized by the actual deployed stent diameter. The position error of stents center was split into a longitudinal distance error e_{cl} along the arterial centerline and a transverse distance error e_t in the plan normal to the centerline.

Results

Qualitative assessment

The simulation results for the three clinical cases are presented in Fig.5A. The superimposition of simulated and real stents, shown in Fig.5B, gives a visual assessment of the results.

In the first clinical case, simulated and post-operative stent locations are nearly identical except for the distal stents of the right iliac limb. These stents and the two stents inside the left iliac aneurysm were not fully deployed; they are smaller in our simulation.

In the second case, simulated and actual stents are well superimposed at the proximal and distal SG ends. However, 75 degrees longitudinal axial rotation of the main aortic body is not reproduced in the simulation.

In the third case, simulated iliac limbs are shorter and distal stents are transversally shifted, while good agreement of aortic body stents position can be observed.

It is also worth mentioning the ability of the simulation to reproduce SG kinks in a realistic manner, as highlighted by the black arrow present in the third case in Fig.5B.

Quantitative comparison

Values of previously defined errors are plotted in Fig.6. Averaged error values for all stents are reported in Table4.

Case #1 presents almost only small values of e_{cl} (mean value is 0.2 ± 1.6 mm). Stents located in the aneurysm sac and at the distal end of the right limb, have the worst position along the centerline (maximum e_{cl} value is 2.9 mm). The values of e_t are rather small and uniformly distributed on all stents (mean value is 2.7 ± 2.2 mm), the maximum transverse position error being in the aneurysm sac. Diameter agreement between simulated and real stents is best at the proximal part of the SG, while distal stents have a higher diameter error e_D, with a maximum error in the left iliac aneurysm (-35.3%).

In case #2, the distal and proximal stents are well positioned longitudinally (less than 2 mm error) whereas the stents inside the aneurysm sac have the worst longitudinal position of all cases (6.5 mm maximum error). The same observation can be made for the transverse error; e_t is small at SG ends and presents a maximum inside the aneurysm sac (e_t rises up to 14.1 mm in this area). As for case #1, most of the simulated stents have the same diameter as the actual stents (e_D ranges between -15 and 0%) and only one distal stent has a rather large diameter error (-35.6%).

In case #3, e_{cl} is between -2.5 and 2.5 mm (mean e_{cl} value is -1.3 ± 2.6 mm), except for the two most distal stents of the main body and the most distal stent of the iliac limb (where e_{cl} maximum is 5.2 mm). The transverse error is lower than in the other cases (2.3 ± 1.3 mm) and reaches 4.9 mm for distal stents. Mean diameter error is -4.9 ± 7.5%, with one single stent presenting a higher e_D value (-23.4%) in the aneurysm sac.

Computation times are presented in Table 3.

Discussion

The present study reports a novel methodology to predict deployment of SGs in patient-specific aneurysm geometries. To our knowledge, this is the first time that several marketed SGs, with all their components, are numerically deployed inside patient-specific AAA models and that the results are validated against post-operative scans. Another original point of this work is the very limited manual intervention on the patient-specific part, thanks to a mesh morphing technique: the final steps of the simulation involving patient-specific data could be automated with previous SG crimping simulation, a pre-operative scan and few other parameters (SG diameters, proximal stent landing position, overlap lengths) as only inputs.

We achieved a qualitative comparison by superimposing simulated and segmented actual stents geometries (Fig.5). In general, this comparison was satisfactory for all cases. Most of simulated stents were at the same location as actual stents. We could observe a slight difference in case #1 where right limb curvature and stent diameter were not exactly the same near the iliac artery bifurcation. This can be explained by incomplete stent expansion in this area. Right iliac arterial wall was not deformed enough by stent expansion and this resulted in a medial deployment of the limb, near the left iliac artery. In case #2, main discrepancies were in the aneurysm sac, while position of stents at SG ends was well predicted. The initial rotation of the prosthesis around its longitudinal axis was not implemented in our simulations. This may explain the large errors (14.1 mm maximum e_t) at the main body stumps and proximal limb extremities. Case #3 is the simulation which showed the best agreement with the post-operative CT scan. Only marginal differences could be noted between simulated and actual SG shapes (especially the two distal stents).

Quantitative results were extracted to confirm the qualitative analysis. Fitting cylinders onto simulated and actual stents allowed us to compare stents center position along centerline's tangent and transverse directions, as well as stents diameter (Fig.6 and Table 4).

In all cases, longitudinal error was less than 2.5 mm for 75% of stents. In cases #1 and #3, maximum longitudinal errors were 2.9 and 5.2 mm, respectively. These errors seem to be due to the fact that arteries were not deformed and straightened enough by the SG. In case #2, stents with the larger error values were all located in the aneurysm sac. This was partly explained by the axial rotation of the main body which was not implemented in the simulation. Another explanation was the lack of mechanical constraints around the SG in the aneurysm sac, particularly the absence of intraluminal thrombus (ILT) modeling. Finally, longitudinal error was reasonable in the perspective of clinical applications (i.e. less than 5 mm). Moreover, it is important to bear in mind that the final error is inherent to the simulation itself but also to pre and post-operative scan registration, stent segmentation and cylinder fitting.

The remarks are quite similar when looking at centerline transverse errors. Mean e_t value was small in case #1 as well as standard deviation (2.7 ± 2.2 mm). High e_t values were seen only in the right iliac limb. Stents at SG ends of case #2 were well positioned radially whereas the actual deployment rotation of the main body induced higher e_t values in the aneurysm sac. In case #3, e_t confirmed the good agreement of simulation and post-operative scan.

In the three simulations, there was good diameter agreement between simulated and real stents. However, simulations seemed to slightly underestimate stent diameters as mean e_D values were all negative (-14.8% to -4.9%). Slightly overestimated AAA material properties may explain such error. In case #1, two stents were not fully deployed inside the left iliac aneurysm, as four distal stents of the right iliac limb. The effect of blood pressure (included within AAA mechanical behavior) may be one reason for

the lack of stent expansion in aneurysm sacs. Local diameter underestimations (as for the right distal stent in case #2) may be related to the fact that SG balloon dilatation was not simulated.

SG longitudinal positioning was well predicted in our simulations. Implementation of this type of simulation in the pre-operative sizing process could help reducing inter-observer variability and increase accuracy of SG design, particularly in complex aortic aneurysms (Banno et al., 2014). Furthermore, assessment of SG kinks and stent apposition defects could assist in the prediction of limb thrombosis or endoleaks.

Limitations

Arterial walls were modeled with constant thickness and mechanical behavior linearized around *in-vivo* loading conditions. This assumption was validated by the good agreement between simulations and post-operative scans. Nevertheless, our simulations could benefit from more sophisticated modeling, including thrombus (Riveros et al., 2015; Toungara and Geindreau, 2013) and calcifications. This could enhance accuracy of SG position in the aneurysm sac. Furthermore, large regional datasets gathered by other research teams (Roccabianca et al., 2014), statistical models (Vande Geest et al., 2006) or novel image processing techniques (Franquet et al., 2013) could enhance arterial wall modeling, with local patient-specific variations.

During simulations, we imposed as only boundary conditions that aortic and iliac extremities were motionless. Further developments could increase biomechanical realism by assigning elastic connectors at the ostias of internal iliac arteries or preventing any posterior displacement near the spine. Blood pressure modeling could also be improved. Fluid-structure interaction analysis would be an appropriate tool to impose pressure loads on both arterial and SG surfaces in contact with the blood. It would also

allow to simulate blood flow following SG deployment (Figueroa et al., 2010) and therefore potential endoleaks.

Finally, we did not intend to extensively reproduce all steps of the EVAR procedure in our simulation. Our goal was rather to predict final SG position with reduced computational costs. The obtained level of accuracy was acceptable from a clinical perspective. However, accuracy of SG position may be further increased by implementing intraoperative steps in the simulation, such as arterial deformation by stiff guidewire and introducer sheath, as well as SG ballooning. Pioneering work on aorto-iliac by stiff guidewire has been recently published by Kaladji et al. (2013).

Conclusion

EVAR is a complex surgery which requires cautious pre-operative planning, from patient selection to stent-graft sizing, in order to prevent post-operative complications and secondary interventions. Within this context, numerical simulations associating patient-specific data and stent-graft modeling could provide information to choose the best-suited device in each case and anticipate complications. Towards this objective, we have proposed a novel computational methodology to predict the deployment of marketed stent-grafts inside patient-specific aneurysms. This strategy was validated on three clinical cases and numerical results showed good agreement with actual post-operative scans. These results emphasize the potential of numerical simulations to improve pre-operative planning of EVAR.

Acknowledgements

The authors would like to acknowledge the Région Rhône-Alpes for the financial support of D. Perrin thesis and the French National Research Agency (ANR) for the funding of Endosim project (grant agreement ANR-13-TECS-0012). 3SR lab is part of the LabEx Tec 21 (Investissements d' Avenir - grant agreement ANR-11-LABX- 0030). We gratefully thank Cemil Goksu (Therenva) and Atul Gupta (Medtronic) for their help and fruitful discussions.

Conflict of interest

The authors have no professional, financial or commercial conflict of interest to declare.

References

Albertini, J.-N., DeMasi, M.-A., Macierewicz, J., El Idrissi, R., Hopkinson, B.R., Clément, C., Branchereau, A., 2005. Aorfix stent graft for abdominal aortic aneurysms reduces the risk of proximal type 1 endoleak in angulated necks: bench-test study. Vascular 13, 321–6.

Albertini, J.N., Macierewicz, J., Yusuf, S.W., Wenham, P.W., Hopkinson, B.R., 2001. Pathophysiology of proximal perigraft endoleak following endovascular repair of abdominal aortic aneurysms: a study using a flow model. European journal of vascular and endovascular surgery 22, 53–6.

Albertini, J.-N., Perdikides, T., Soong, C., Hinchliffe, R., Trojanowska, M., Yusuf, S., Clément, C., Hopkinson, B.R., 2006. Endovascular repair of abdominal aortic aneurysms in patients with severe angulation of the proximal neck using a flexible stent-graft: European Multicenter Experience. Journal of cardiovascular surgery 47, 245–250.

Auricchio, F., Conti, M., De Beule, M., De Santis, G., Verhegghe, B., 2011. Carotid artery stenting simulation: from patient-specific images to finite element analysis. Medical engineering & physics 33, 281–9.

Auricchio, F., Conti, M., Marconi, S., Reali, a, Tolenaar, J.L., Trimarchi, S., 2013. Patient-specific aortic endografting simulation: From diagnosis to prediction. Computers in biology and medicine 43, 386–94.

Auricchio, F., Taylor, R.L., 1997. Shape-memory alloys : modelling and numerical simulations the finite-strain superelastic behavior. Computer Methods in Applied Mechanics and Engineering 143, 175–194.

Banno, H., Kobeiter, H., Brossier, J., Marzelle, J., Presles, E., Becquemin, J.-P., 2014. Inter-observer variability in sizing fenestrated and/or branched aortic stent-grafts. European journal of vascular and endovascular surgery 47, 45–52.

Carroccio, A., Faries, P.L., Morrissey, N.J., Teodorescu, V., Burks, J., Gravereaux, E.C., Hollier, L.H., Marin, M.L., 2002. Predicting iliac limb occlusions after bifurcated aortic stent grafting: Anatomic and device-related causes. Journal of Vascular Surgery 36, 679–684.

Cochennec, F., Becquemin, J.P., Desgranges, P., Allaire, E., Kobeiter, H., Roudot-Thoraval, F., 2007. Limb Graft Occlusion Following EVAR : Clinical Pattern , Outcomes and Predictive Factors of Occurrence. European Journal of endovascular surgery 65, 59–65.

De Bock, S., Iannaccone, F., De Beule, M., Van Loo, D., Vermassen, F., Verhegghe, B., Segers, P., 2013. Filling the void: a coalescent numerical and experimental technique to determine aortic stent graft mechanics. Journal of biomechanics 46, 2477–82.

De Bock, S., Iannaccone, F., De Santis, G., De Beule, M., Van Loo, D., Devos, D., Vermassen, F., Segers, P., Verhegghe, B., 2012. Virtual evaluation of stent graft deployment: a validated modeling and simulation study. Journal of the mechanical behavior of biomedical materials 13, 129–39.

Demanget, N., Avril, S., Badel, P., Orgéas, L., Geindreau, C., Albertini, J.-N., Favre, J.-P., 2012a. Computational comparison of the bending behavior of aortic stent-grafts. Journal of the mechanical behavior of biomedical materials 5, 272–82.

Demanget, N., Duprey, A., Badel, P., Orgéas, L., Avril, S., Geindreau, C., Albertini, J.-N., Favre, J.-P., 2013. Finite element analysis of the mechanical performances of 8 marketed aortic stent-grafts. Journal of endovascular therapy : an official journal of the International Society of Endovascular Specialists 20, 523–35.

Demanget, N., Latil, P., Orgéas, L., Badel, P., Avril, S., Geindreau, C., Albertini, J.-N., Favre, J.-P., 2012b. Severe bending of two aortic stent-grafts: an experimental and numerical mechanical analysis. Annals of biomedical engineering 40, 2674–86.

Figueroa, C.A., Taylor, C.A., Yeh, V., Chiou, A.J., Gorrepati, M.L., Zarins, C.K., 2010. Preliminary 3D computational analysis of the relationship between aortic displacement force and direction of endograft movement. Journal of vascular surgery 51, 1488–97; discussion 1497.

Franquet, A., Avril, S., Le Riche, R., Badel, P., Schneider, F.C., Li, Z.Y., Boissier, C., Favre, J.P., 2013. A new method for the in vivo identification of mechanical properties in arteries from cine MRI images: theoretical framework and validation. IEEE transactions on medical imaging 32, 1448–61.

Gasser, T.C., Ogden, R.W., Holzapfel, G. a, 2006. Hyperelastic modelling of arterial layers with distributed collagen fibre orientations. Journal of the Royal Society 3, 15–35.

Georgakarakos, E., Xenakis, A., Georgiadis, G.S., Argyriou, C., Antoniou, G. a, Schoretsanitis, N., Lazarides, M.K., 2014. The hemodynamic impact of misalignment of fenestrated endografts: a computational study. European journal of vascular and endovascular surgery 47, 151–9.

Greenhalgh, R.M., Brown, L.C., Powell, J.T., Thompson, S.G., Epstein, D., Sculpher, M.J., 2010. Endovascular versus open repair of abdominal aortic aneurysm. The New England journal of medicine 362, 1863–71.

Haskett, D., Johnson, G., Zhou, A., Utzinger, U., Vande Geest, J., 2010. Microstructural and biomechanical alterations of the human aorta as a function of age and location. Biomechanics and modeling in mechanobiology 9, 725–36.

Holzapfel, G.A., Stadler, M., Gasser, T.C., 2005. Changes in the mechanical environment of stenotic arteries during interaction with stents: computational assessment of parametric stent designs. Journal of biomechanical engineering 127, 166–80.

Horný, L., Netušil, M., Voňavková, T., 2013. Axial prestretch and circumferential distensibility in biomechanics of abdominal aorta. Biomechanics and modeling in mechanobiology 783–799.

Howell, B.A., Kim, T., Cheer, A., Dwyer, H., Saloner, D., Chuter, T.A.M., 2007. Computational fluid dynamics within bifurcated abdominal aortic stent-grafts. Journal of Endovascular Therapy 14, 138–43.

Kaladji, A., Dumenil, A., Castro, M., Cardon, A., Becquemin, J.-P., Bou-Saïd, B., Lucas, A., Haigron, P., 2013. Prediction of deformations during endovascular aortic aneurysm repair using finite element simulation. Computerized medical imaging and graphics 37, 142–9.

Kleinstreuer, C., Li, Z., Basciano, C. a, Seelecke, S., Farber, M. a, 2008. Computational mechanics of Nitinol stent grafts. Journal of biomechanics 41, 2370–8.

Kochanek, K.D., Xu, J., Murphy, S.L., Minin, A.M., 2011. Deaths: final data for 2009. National Vital Statistics Reports 60.

Layman, R., Missoum, S., Geest, J. Vande, 2010. Simulation and probabilistic failure prediction of grafts for aortic aneurysm. Engineering Computations 27, 84–105.

Li, Z., Kleinstreuer, C., 2006. Analysis of biomechanical factors affecting stent-graft migration in an abdominal aortic aneurysm model. Journal of biomechanics 39, 2264–73.

Molony, D.S., Kavanagh, E.G., Madhavan, P., Walsh, M.T., McGloughlin, T.M., 2010. A computational study of the magnitude and direction of migration forces in patient-specific abdominal aortic aneurysm stent-grafts. European journal of vascular and endovascular surgery 40, 332–9.

Mortier, P., Holzapfel, G. a, De Beule, M., Van Loo, D., Taeymans, Y., Segers, P., Verdonck, P., Verhegghe, B., 2010. A novel simulation strategy for stent insertion and deployment in curved coronary bifurcations: comparison of three drug-eluting stents. Annals of biomedical engineering 38, 88–99.

Perrin, D., Demanget, N., Badel, P., Avril, S., Orgéas, L., Geindreau, C., Albertini, J.-N., 2015. Deployment of stent grafts in curved aneurysmal arteries: toward a predictive numerical tool. International journal for numerical methods in biomedical engineering 31, 26–36.

Prasad, A., Xiao, N., Gong, X.-Y., Zarins, C.K., Figueroa, C.A., 2013. A computational framework for investigating the positional stability of aortic endografts. Biomechanics and modeling in mechanobiology 12, 869–87.

Riveros, F., Martufi, G., Gasser, T.C., Rodriguez-Matas, J.F., 2015. On the Impact of Intraluminal Thrombus Mechanical Behavior in AAA Passive Mechanics. Annals of biomedical engineering.

Roccabianca, S., Figueroa, C. a, Tellides, G., Humphrey, J.D., 2014. Quantification of regional differences in aortic stiffness in the aging human. Journal of the mechanical behavior of biomedical materials 29, 618–34.

Sternbergh, W.C., Carter, G., York, J.W., Yoselevitz, M., Money, S.R., 2002. Aortic neck angulation predicts adverse outcome with endovascular abdominal aortic aneurysm repair. Journal of vascular surgery 35, 482–6.

Toungara, M., Geindreau, C., 2013. Influence of a Poro-Mechanical Modeling of the Intra-Luminal Thrombus and the Anisotropy of the Arterial Wall on the Prediction of the Abdominal Aortic Aneurysm Rupture. Cardiovascular Engineering and Technology 4, 192–208.

Vad, S., Eskinazi, A., Corbett, T., McGloughlin, T., Vande Geest, J.P., 2010. Determination of coefficient of friction for self-expanding stent-grafts. Journal of biomechanical engineering 132, 121007.

Vande Geest, J.P., Wang, D.H.J., Wisniewski, S.R., Makaroun, M.S., Vorp, D. a, 2006. Towards a noninvasive method for determination of patient-specific wall strength distribution in abdominal aortic aneurysms. Annals of biomedical engineering 34, 1098–106.

Fig 1: Pre-operative scans (A), corresponding arterial wall meshes (B) and pre-stressed models of the various SG components used during EVAR (C) for the three clinical cases

Fig 2: Consecutive steps involving finite-element analysis: Main body and limbs crimping and relative positioning (A); SG insertion and positioning in the tubular shape (B); Mesh morphing from tubular shape to actual pre-operative geometry (C); Mechanical equilibrium between SG and arteries (D)

Fig 3: Representative evolution of the ratio of the kinetic energy divided by the total energy along the deployment simulation, for case #1. 1: First contact between SG and morphed AAA. 2: morphing step. 3: Beginning of the mechanical equilibrium simulation step.

Fig 4: Stents segmentation on the post-operative scan (A) and cylinder fitting (red) on these segmented stents (black) (B)

Fig 5: Simulation results (A) and qualitative comparison of the geometry of simulated (red) and actual (white) deployed SGs (B) for the three clinical cases

Fig 6: Stent by stent errors for the three clinical cases: longitudinal position errors (e_{cl}) along the vessel centerline (A), transverse position errors (e_t) perpendicularly to the centerline (B) and relative diameter errors (e_D) (C). Each square is one stent; columns are representing different SG components. The error for each stent is coded by the color of the square. White squares represent stents which were not included in the statistics due to impossible segmentation on the post-operative scan. Crossed squares were not included in diameter statistics due to their elliptic shape.

Table 1: Clinical summary of the three EVAR procedures

Table 2: Parameters of hyperelastic Holzapfel-Gasser-Ogden model used for linearization and in-plane parameters of linearized orthotropic model

Table 3: Time parameters of all steps involving FEA and corresponding computation times, for the three clinical cases. Time step is the length of the step prescribed to Abaqus. Time increment is the targeted increment, achieved using mass scaling. CPU time reflects the time a single processor would require computing the simulation. Real time reflects the real time required computing the simulation on our 12 processors setup.

Table 4: Mean, standard and maximum errors over all stents of the SG for each clinical case. The two crossed squares of Fig 6 were not included in diameter statistics due to their elliptic shape.

Fig 1

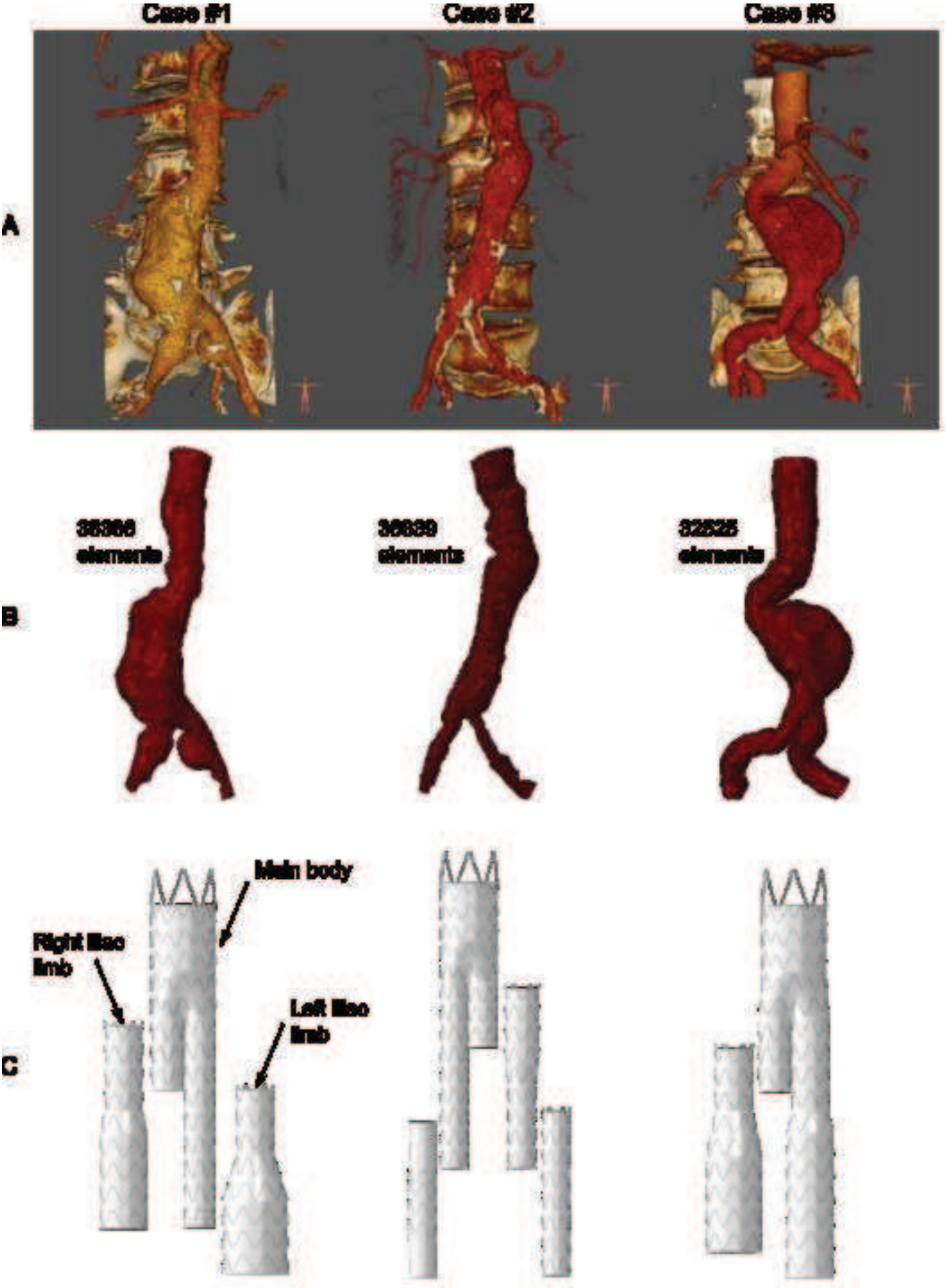

Fig 2

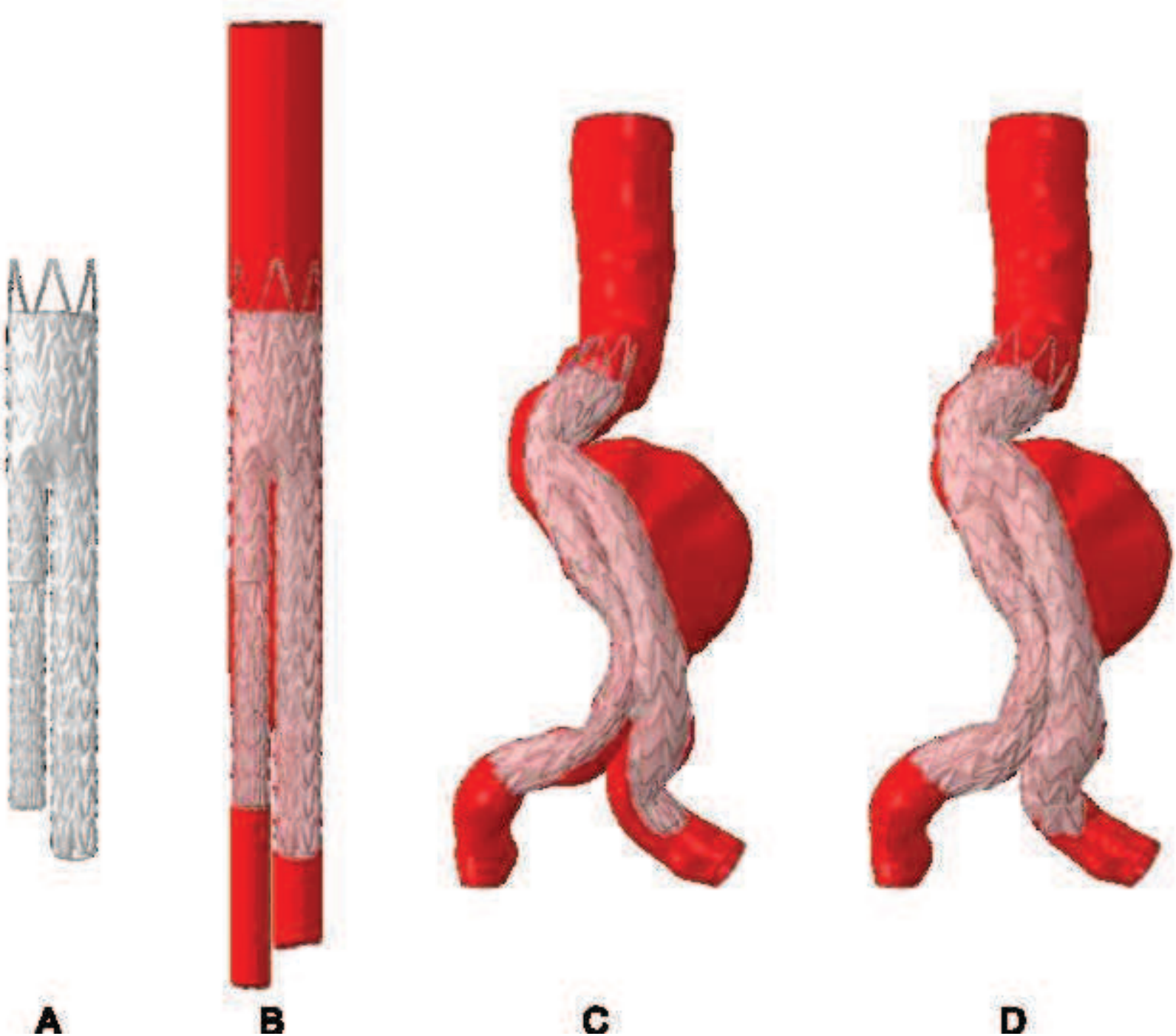

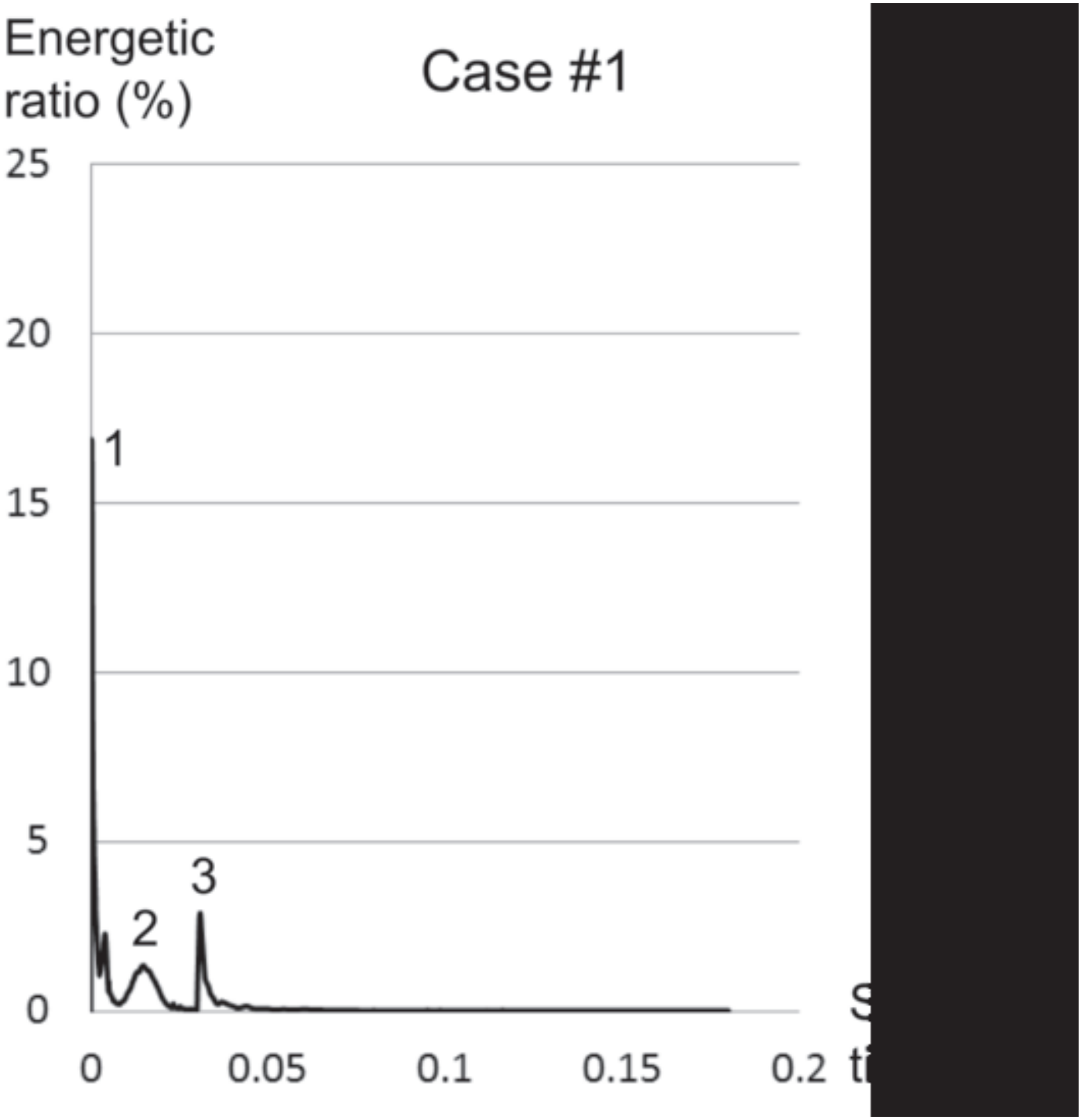

Fig 5

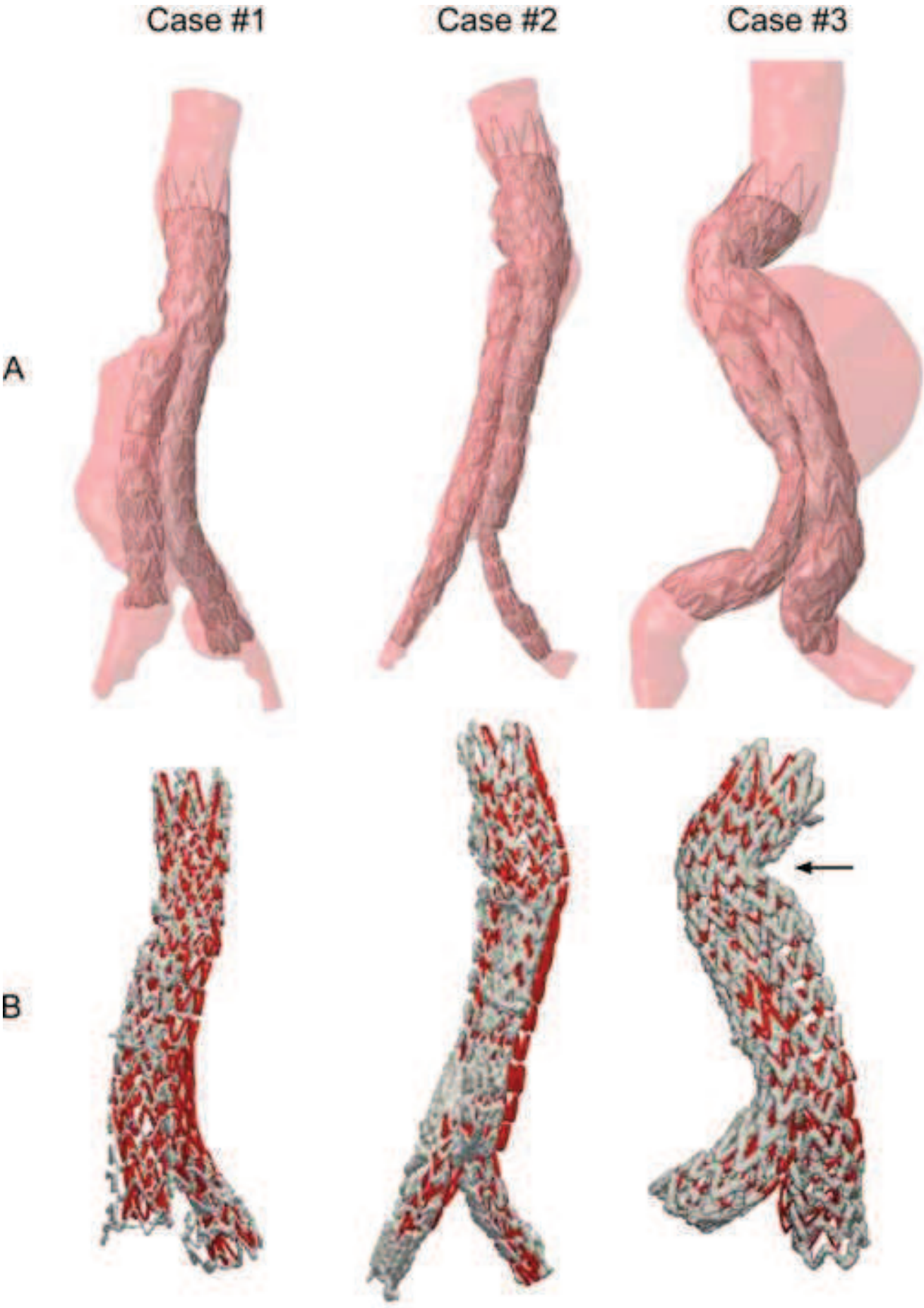

Fig 6

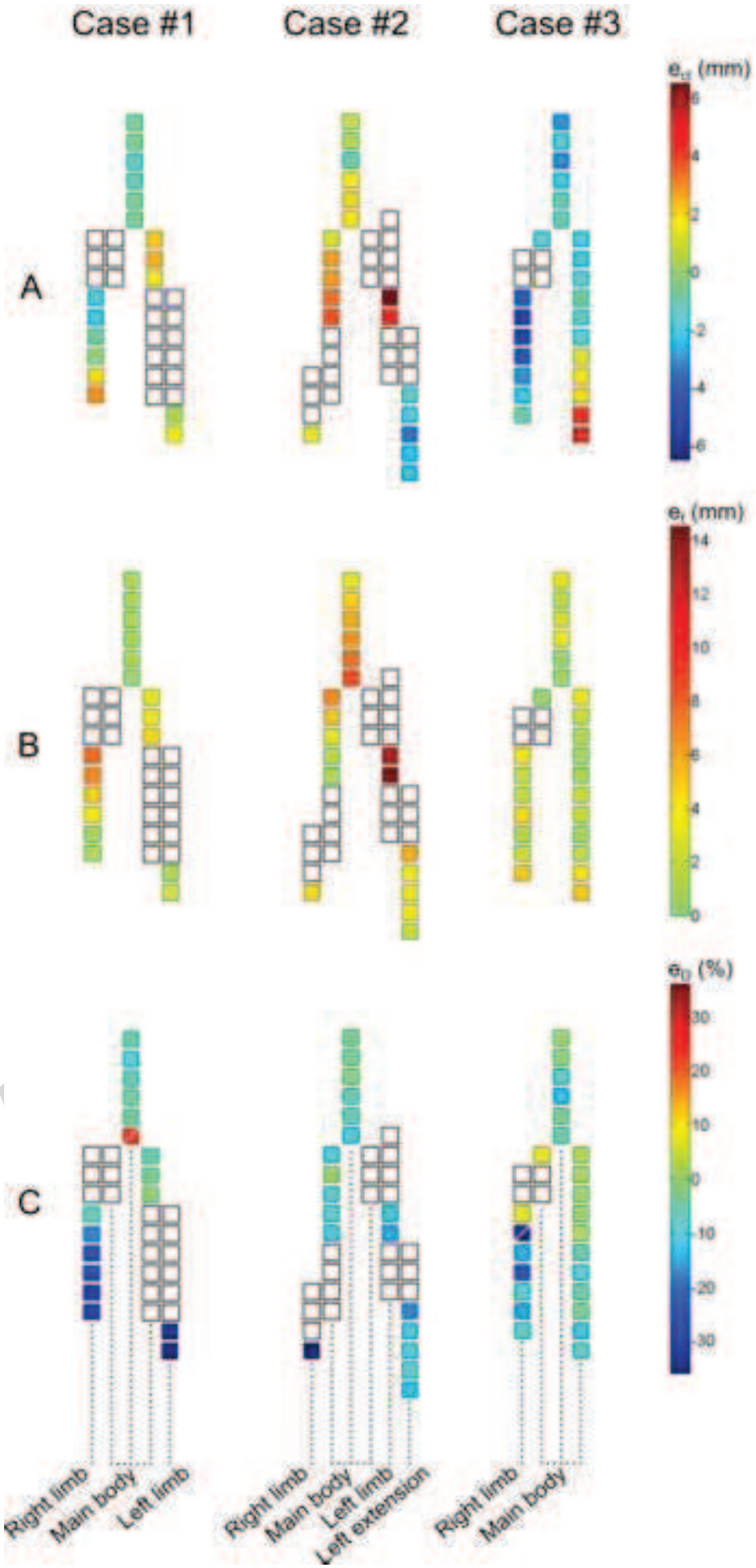
Case #1
Case #2
Case #3
A
B
C
e_{zz} (mm)
6
4
2
0
-2
-4
-6
e_t (mm)
14
12
10
8
6
4
2
0
e_D (%)
30
20
10
0
-10
-20
-30
Right limb
Main body
Left limb
Right limb
Main body
Left limb
Left extension
Right limb
Main body

Table 1

	Case #1	Case #2	Case #3
Age (y)	70	58	78
Sex	Male	Male	Male
Stent-graft: Main body Right limb Left limb Left extension	 ENBF-28-13-C-145-EE ENLW-16-20-C-95-EE ENLW-16-28-C-80-EE None	 ENBF-28-13-C-145-EE ZSLE-13-56-ZT ENLM-16-13-C-95-EE ENEW-13-13-C-80-EE	 ENBF-28-20-C-170-EE ENLW-16-24-C-95-EE None None
Aorto-iliac anatomy and SG deployment features	Left and right iliac aneurysms	Main body rotated by 75° around the longitudinal axis	60° angulated AAA neck
Aneurysm sac thrombus	Length: 60 mm Maximum thickness: 20 mm	Length: 100 mm Maximum thickness: 20 mm	None

Table 2

Parameters and values of hyperelastic Holzapfel-Gasser-Ogden model:		
c_{10} (MPa)	Stress-like material parameter	100.9
k_1 (GPa)	Stress material parameter	4.07
k_2	Dimensionless parameter	165.55
κ	Level of dispersion parameter	0.16
θ (°)	Fiber orientation angle	48.4
K (GPa)	Bulk modulus	75.5
In-plane parameters and values of linearized orthotropic linear elastic model:		
E_z (MPa)	Elastic modulus along vessel centerline	3.58
E_θ (MPa)	Elastic modulus along vessel circumferential direction	1.11
$\nu_{\theta z}$	Arterial wall in-plane minor Poisson ratio	0.44
$G_{z\theta}$ (MPa)	Arterial wall in-plane shear modulus	4.0

Table 3

		Simulation parameters		Computation times	
		Time step (s)	Time increment (s)	CPU time (h)	Real time (h)
Case #1					
	SG assembling and crimping	0.04	5E-8	199:00	16:35
	Deployment in the preoperative geometry	0.03	3E-8	147:00	12:15
	Mechanical equilibrium	0.15	3E-8	845:00	70:25
Case #2					
	SG assembling and crimping	0.05	4E-8	282:00	23:30
	Deployment in the preoperative geometry	0.07	4E-8	266:00	22:10
	Mechanical equilibrium	0.15	4E-8	534:00	44:30
Case #3					
	SG assembling and crimping	0.017	5E-8	84:00	7:00
	Deployment in the preoperative geometry	0.03	5E-8	113:00	9:25
	Mechanical equilibrium	0.15	5E-8	474:00	39:20

Table 4

	Case #1	Case #2	Case #3
Stents position error along the centerline (mm):			
Mean ± standard deviation	0.2 ± 1.6	1.1 ± 2.6	-1.3 ± 2.6
Maximum	2.9	6.5	5.2
Stents position error perpendicularly to the centerline (mm):			
Mean ± standard deviation	2.7 ± 2.2	5.4 ± 3.5	2.3 ± 1.3
Maximum	7.7	14.1	4.9
Stents diameter relative error (%):			
Mean ± standard deviation	-14.8 ± 12.5	-10.2 ± 7.8	-4.9 ± 7.5
Maximum	-35.3	-35.6	-23.4